A model for the formation of gold nanoparticles in the citrate synthesis method

Emmanuel Agunloye, Luca Panariello, Asterios Gavriilidis, Luca Mazzei *

Department of Chemical Engineering, University College London, Torrington Place, WC1E 7JE, UK

HIGHLIGHTS

- A new mathematical model for the citrate synthesis method of gold nanoparticles has been developed.
- The model is based on the "seed-mediated" mechanistic description of the synthesis.
- This mechanistic description accounts for the acid-base properties of the synthesis precursor and reducing agent.
- The predicted final mean sizes of the nanoparticles closely agree with those measured experimentally.

ABSTRACT

This paper presents a new model for predicting the evolution of the particle size of gold nanoparticles (GNPs) in the citrate synthesis method. In this method, the precursor is an acid solution of tetrachloroauric acid, while the reducing agent is a base solution of sodium citrate. The acid-base properties of the solutions influence how the size of the particles evolves during the synthesis. In the literature, various mechanistic theories have been proposed to explain this evolution. Turkevich et al. (1951), who pioneered this synthesis method, suggested the "organizer theory". This mechanistic description of the synthesis was modelled by Kumar et al. (2007), but recently Agunloye et al. (2017) showed that in several cases this model performed poorly, since it does not account for the acid-base properties of the reactants. In this work, we present a kinetic model based on the synthesis seed-mediated mechanistic description proposed by Wuithschick et al. (2015). In this description, the precursor concurrently reduces into gold atoms and hydroxylates into a passive form. The gold atoms then aggregate into seed particles, which finally react with the passive form of the precursor in a growth step. We validated the model using experimental data from the literature obtained for conditions in which the seed-mediated mechanism is valid. The predicted GNP final sizes closely agree with those obtained experimentally.

1. Introduction

Gold nanoparticles (GNPs) have applications in a variety of fields. In biomedicine, for example, they are used in cancer diagnosis and biological imaging. GNPs possess excellent catalytic properties and high conductivity, which can be tuned using particle size, surface functionality and intraparticle separation. Such properties are exploited in many electrochemical and electrocatalytic sensors. Their optical, optoelectronic, electrochemical and electrocatalytic properties are used to detect biomolecules such as proteins, DNA, oligonucleotides, pathogens, and also entire cancer cells; this has significant impact in healthcare applications (Yang et al., 2015;

Dreaden et al., 2012; Zhang et al., 2014; Lane et al., 2015; Matias et al., 2017; Zhou et al., 2015). Even if bulk gold is inert, in nanoparticle form it displays high catalytic activity for a variety of reactions, such as oxidations of olefins, alcohols and alkanes, hydrogenations, and aminations (Corma and Garcia, 2008; Daniel and Astruc, 2004; Stratakis and Garcia, 2012). Geometrical properties, such as size and shape, determine how the particles perform. When the GNP size approaches the Fermi wavelength of electrons (<2 nm), molecule-like optical properties and size-dependent fluorescence appear (Zhou et al., 2015; Yang et al., 2015). Large GNPs have a longer electromagnetic field decay length and provide higher sensitivity; so, they are more efficient at enhancing Raman signals (Yang et al., 2015). In catalysis, the size of the GNPs strongly influences their performance. Catalytic activity of GNPs typically increases substantially as size decreases below 5 nm (e.g. CO

oxidation). However, selectivity to desired products can increase or decrease with nanoparticle size, depending on the particular reaction (Hvolbæk et al., 2007; Hashmi and Hutchings, 2006).

Spherical GNPs with sizes from 10 to 150 nm can be produced via a synthetic route known as *the citrate method*. Many authors have explored this method for different applications and have investigated how the nanoparticles form when the precursor (a tetrachloroauric acid solution) reacts with the reducing agent (a trisodium citrate solution). However, the GNPs produced are usually polydisperse and irreproducible. Sometimes, the polydispersity can be ~40% (Ji et al., 2007), therefore undermining product quality. A model of the synthesis would help to select the conditions in which to produce the nanoparticles and to design the reactor in which the synthesis is to be conducted; this would allow controlling the process better and rendering the particles more reproducible.

In the past, researchers explained the GNPs synthesis through the pioneering work of Turkevich et al. (1951), who suggested that the particles form via a nucleation-growth mechanism. According to this mechanistic description of the synthesis, tetrachloroauric acid reacts with sodium citrate to form gold chloride and dicarboxy acetone (DCA). Subsequently, the latter (which acts as nucleation agent) organizes gold chloride to form gold nuclei, while decomposing into acetone. Its decomposition eventually prevents the generation of new nuclei (nucleation stops), leaving behind unconsumed gold chloride that reacts on the surface of the particles thereby making them grow. Nucleation and growth are therefore decoupled.

Kumar et al. (2007) developed a mathematical model for the description of the GNPs synthesis, basing it on such a theory. In our recent work (Agunloye et al., 2017), we tested the model for different synthesis conditions studied experimentally by various researchers, for which results are available in the literature. The model poorly predicted the experimental data, because the Turkevich organizer theory does not account for the acid-base properties of the precursor and reducing agent.

In the last decade, however, new evidence has emerged indicating that the particles aggregate significantly during the synthesis, aggregation taking place after nucleation but before growth (Wuithschick et al., 2015). Further evidence has shown that changing the pH value at which the synthesis is conducted affects the processes of nucleation, aggregation and growth, and influences the final size of the particles (Ji et al., 2007). For example, the effect of aggregation, which occurs significantly at low pH values, decreases when the pH increases, while an opposite trend is found for growth. This behaviour is due to the chemistry of the precursor and reducing agent, which are a strong acid and a weak base, respectively. In addition, both of them exist in different forms depending on the value of the mixture pH: the precursor can exist as $AuCl_4^-$, $AuCl_3(OH)^-$, $AuCl_2(OH)_2^-$, $AuCl(OH)_3^-$ and $Au(OH)_4^-$, whilst the reducing agent can exist as Ct^{3-}, CtH^{2-}, CtH_2^- and CtH_3. Only pH values between 3 and 8, measured at room temperature, favour the synthesis (Ji et al., 2007). While investigating the synthesis within this pH range, Wuithschick et al. (2015) proposed the so-called "seed-mediated mechanism", in which nuclei generate "seed particles", which then grow into the particles of final size.

In this paper, we develop a new model for the synthesis based on the seed-mediated mechanism. This mechanism originates from the thermodynamics and kinetics of the synthesis. Thermodynamics allows identifying the chemical components and their amounts at quasi-equilibrium and final equilibrium states (later on, we will explain the concept of quasi-equilibrium in the context of the citrate synthesis method). Kinetics, on the other hand, provides the rates of the reactions involved in the synthesis. In developing the model, we take into account the thermodynamics of the substances involved in the synthesis. Then, we derive rate-order equations for the reactions that occur in the pH range of interest for the synthesis analysed. To predict the evolution of concentrations and particle size distribution, we derive mass balance equations for the fluid components and a population balance equation (PBE) for the GNPs. These describe the synthesis according to the seed-mediated mechanism of Wuithschick et al. (2015). While the mass balance equations are ordinary differential equations, the PBE is an integro-partial differential equation. Their combination yields a complex model that can only be solved numerically. To solve it, we employ the commercial numerical code Parsival. For the initial conditions, we adopt the process conditions that other researchers previously used in this synthesis method to produce GNPs. We then compare the model predictions to experimental data from literature.

The article is structured as follows. Section 2 briefly presents the seed-mediated mechanism. Section 3 reports the reactions that occur in the synthesis according to this mechanism, their corresponding rate-order equations and the balance equations for the components. Section 4 presents the solutions of the model and discusses the results. Finally, Section 5 reports the conclusions of the work.

2. Seed-mediated mechanism

In this section, we describe how gold nanoparticles evolve in the citrate synthesis method according to the seed-mediated mechanism of Wuithschick et al. (2015). For this synthesis, two solutions are prepared, one containing tetrachloroauric acid and the other containing sodium citrate in water. The aqueous medium renders the acid-base properties of precursor and reducing agent possible, dissociating according to the following equilibrium reaction:

$$H_2O \rightleftarrows H^+ + OH^- \qquad (2.1)$$

At 25 °C, the equilibrium constant $K_{a,w}$ of the dissociation of water, expressed as $K_{a,w} = C_{H^+} \cdot C_{OH^-}$, is equal to 10^{-14} (Sandler, 2006), where C_{H^+} and C_{OH^-} denote the concentrations of H^+ and OH^-, respectively, measured in mol/dm^3 (here and below, C denotes the molar concentration of a reactant, in the units just given, the subscript indicating the component being considered). The acid-base property of an aqueous medium is usually indicated by the value of the pH, expressed as $pH \equiv -\log_{10} C_{H^+}$. In distilled water, $C_{H^+} = C_{OH^-}$. Hence, for distilled water at 25 °C, $pH = 7$, which is regarded as the neutral pH. The value of the neutral pH, nevertheless, changes with temperature, because $K_{a,w}$ is temperature-dependent. For example, at the standard synthesis temperature of 100 °C, the value of the neutral pH is 5.6.

Apart from Eq. (2.1), in the precursor solution, tetrachloroauric acid, which is a strong acid, completely ionizes according to:

$$HAuCl_4 \rightarrow H^+ + AuCl_4^- \qquad (2.2)$$

The H^+ ions produced in Eq. (2.2) shift the equilibrium position of Eq. (2.1) to the left so that the amount of OH^- ions present in the solution is negligible. So, even if OH^- can hydroxylate $AuCl_4^-$ to the species $AuCl_3(OH)^-$, $AuCl_2(OH)_2^-$, $AuCl(OH)_3^-$ and $Au(OH)_4^-$, their equilibrium amounts in the precursor solution are negligible. To illustrate this, we present a sample calculation in Appendix A (Section A.1) of the supporting information (SI). So, in the tetrachloroauric solution, the precursor exists almost entirely as $AuCl_4^-$ and the pH of this solution is equal to $-\log_{10} C_{HAuCl_4}$.

On the other hand, the reducing agent solution of sodium citrate is a base solution that contains a significant amount of

OH$^-$ because citrate consumes H$^+$ ions and shifts the equilibrium of Eq. (2.1) to the right according to the following reactions:

$$Na_3Ct \rightarrow 3Na^+ + Ct^{3-} \tag{2.3}$$

$$Ct^{3-} + H^+ \rightleftarrows CtH^{2-}; 1/K_{R3} \tag{2.4}$$

$$CtH^{2-} + H^+ \rightleftarrows CtH_2^-; 1/K_{R2} \tag{2.5}$$

$$CtH_2^- + H^+ \rightleftarrows CtH_3; 1/K_{R1} \tag{2.6}$$

where the K_{Ri}'s are the equilibrium constants of the reactions reported, whose values at 25 °C are $7.41 \times 10^{-4}, 1.74 \times 10^{-5}$ and 3.98×10^{-7}, respectively (Serjeant and Dempsey, 1979). Because the amount of OH$^-$ ions is larger than that of H$^+$ ions, the value of the pH of the reducing agent solution is above 7 at 25 °C. To illustrate this, we present a sample calculation in Appendix A (Section A.2) of the SI.

Upon adding the reducing agent solution to the precursor solution in the synthesis, usually carried out at 100 °C in a well-mixed batch reactor, a number of reactions can occur at different rates. For example, Pines et al. (1997) reported $\sim 10^{-11}$ s as the time scale for reactions involving H$^+$ ions to reach completion at 23 °C. Hence, we expect the equilibrium reactions in Eqs. (2.1) and (2.4)–(2.6) to occur almost instantaneously. Wuithschick et al. (2015) confirmed this expectation experimentally: they reported that the reactions attain equilibrium in less than 2 s at 23 °C (notice that the time resolution of the instrument that they used was of seconds). Because of these fast reactions (fast compared to the other reactions involved in the synthesis), the synthesis mixture reaches a temporary equilibrium state, henceforth referred to as "quasi-equilibrium" state, before other reactions begin to occur significantly. When this state is reached, the amount of OH$^-$ is significant and can convert AuCl$_4^-$ into the hydroxylated forms previously reported. To illustrate this, we provide a sample calculation in Appendix A (Section A.3) of the SI.

The speciation of chloroauric acid can in principle yield various hydroxylated species, namely, AuCl$_3$(OH)$^-$, AuCl$_2$(OH)$_2^-$, AuCl(OH)$_3^-$ and Au(OH)$_4^-$. Peck et al. (1991) investigated the speciation reactions of the precursor solution using both UV–vis and Raman spectroscopy and reported that below a pH value of 6.2 (measured at about 25 °C) AuCl$_4^-$ is the dominant species, whilst in the pH range 6.2–8.4 AuCl$_4^-$ and AuCl$_3$(OH)$^-$ dominate. At larger values of the pH, the higher hydroxylated species dominate, starting with AuCl$_2$(OH)$_2^-$ and then moving to the others in succession. So, we assume that within the pH range 3–8, in which the synthesis is conducted, OH$^-$ only hydroxylates AuCl$_4^-$ into AuCl$_3$(OH)$^-$. Referred to as "passivation step", this reaction occurs significantly over a time scale of ~ 30 s at 100 °C (Wuithschick et al., 2015).

Moreover, AuCl$_4^-$ (gold oxidation state of +3) converts into Au (gold oxidation state of zero) by the reducing action of the sodium citrate solution; this occurs significantly over a time scale similar to that characterizing the passivation reaction at 100 °C (Wuithschick et al., 2015). Therefore, after a time of about a minute, all the gold initially present in the precursor is (prevalently) either in the form of atomic gold or of AuCl$_3$(OH)$^-$. In the remaining 20 min of the synthesis, all the gold converts into nanoparticles, as reported by researchers such as Ji et al. (2007), Frens (1973) and Wuithschick et al. (2015).

To understand the mechanism of the synthesis, Polte et al. (2010) and Wuithschick et al. (2015) investigated it using a combination of small-angle X-ray scattering and X-ray absorption near-edge structure along with the other conventional techniques of transmission electron microscopy, surface electron microscopy and UV–vis. This equipment provides time-resolved in situ
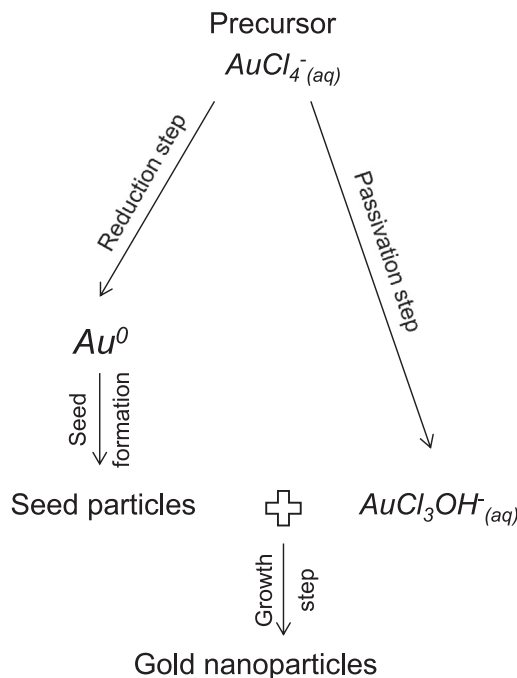

Fig. 2.1. Reaction scheme in the seed-mediated synthesis mechanism describing how the gold in the precursor evolves into GNPs in the citrate synthesis method.

information on the size of nanoparticles of about 2 nm or larger and of their number concentration, offering a reliable account of the synthesis. For the synthesis carried out at 75 °C, Polte et al. (2010) reported this information for a total synthesis time of 80 min (in Fig. 2(d) of their article). We have reproduced this figure in Fig. B.1 in Appendix B of the SI. From this figure, we see that in the time interval between 20 and 80 min the aggregation process is absent, because the particle number concentration is constant. Before 20 min, however, the aggregation process is present, because the number concentration of particles decreases. To determine whether the growth process is also present before this time, we further analysed Fig. B.1. From this analysis, reported in Appendix B (Section B.1) of the SI, we can state that the growth process is nearly insignificant before this time. So, in developing a mathematical model, it can be assumed that in the synthesis the aggregation process is entirely decoupled from the growth process. According to Wuithschick et al. (2015), the nanoparticles stop aggregating when they reach about the same size, which is referred to as "seed" size. Then, these "seed particles" grow into the final NPs by reacting with the hydroxylated precursor, which we assume to be in the form of AuCl$_3$(OH)$^-$ considering the pH range of interest in the citrate synthesis method. Based on these explanations, we present the seed-mediated mechanism as shown in Fig. 2.1. AuCl$_4^-$ passivates into AuCl$_3$(OH)$^-$ and concurrently reduces into atomic gold. As gold atoms generate, they aggregate forming particle seeds; growth is not entirely absent, but its contribution is much less significant and thus is neglected. Finally, the gold present in AuCl$_3$(OH)$^-$ grows the seeds into NPs; during this step aggregation is absent.

3. Model development

In this section, we derive a model for the GNP citrate synthesis based on the seed-mediated mechanism as presented in Fig. 2.1. The precursor solution is mixed with the reducing agent solution to form the *synthesis solution*, where GNPs then form. The reduction, passivation and growth steps involve chemical reactions,

while the seed formation step involves solely the aggregation process. For the chemical reactions, we first derive balanced chemical equations and then develop their rate equations, whilst for the seed formation step we suggest a method for calculating the seed diameter that is applicable for initial molar ratios of sodium citrate to gold (more precisely to tetrachloroauric acid) equal to or greater than five. For initial molar ratios with these values, as illustrated in Appendix C of the SI, the values of the pH of the synthesis solution at quasi and final equilibrium are approximately equal. Based on this observation, we derive a model for the synthesis.

3.1. Precursor reduction step

In the reduction step $AuCl_4^-$ converts into gold atoms owing to the reducing action of the sodium citrate solution. As a result of the speciation reactions of citrate, given by Eqs. (2.4)–(2.6), the reducing agent can be Ct^{3-}, CtH^{2-}, CtH_2^-, CtH_3 or a combination thereof. Using molecular thermodynamic simulations, Ojea–Jimenez and Campanera (2012) reported that the reducing agent is CtH_2^-, while Kettemann et al. (2016) suggested that it is CtH^{2-}. We tested both alternatives, using data about the kinetics of the synthesis reported by Ji et al. (2007). From this test, we concluded that CtH_2^- is the most likely form of the reducing agent, as discussed in Appendix D (Section D.3) of the SI.

For the conversion of the precursor into gold atoms, Kumar et al. (2007) reported the overall balanced chemical equation in the form:

$$2AuCl_3 + 3[(COO^-CH_2)_2C(OH)COO^-] + 3H^+ \rightarrow 2Au^0 + 3(CH_3)_2C=O + 9CO_2 + 6Cl^- \tag{3.1}$$
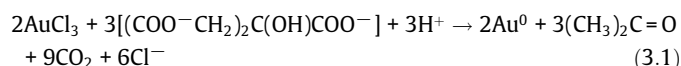
In this equation, $AuCl_3$ appears as precursor and Ct^{3-} as reducing agent. However, several authors, such as Ji et al. (2007) and Wuithschick et al. (2015), do not report the reaction in this form because, as said in Section 2, in the precursor solution gold is in the form of $AuCl_4^-$. Substituting $AuCl_3$ with $AuCl_4^- - Cl^-$ and Ct^{3-} with $CtH_2^- - 2H^+$, we can express Eq. (3.1) in terms of $AuCl_4^-$ and CtH_2^-. Rearranging the chemical species as reactants and products yields:

$$2AuCl_4^- + 3(CH_2COOH)_2C(OH)COO^- \rightarrow 2Au^0 + 8Cl^- + 3(CH_3)_2C=O + 9CO_2 + 3H^+ \tag{3.2}$$
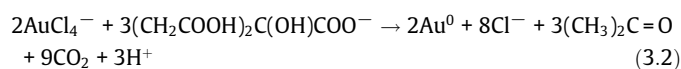
Eq. (3.2) is the balanced chemical equation for the reduction step. The stoichiometry of this reaction requires three moles of CtH_2^- to reduce two moles of $AuCl_4^-$.

We assume that the kinetics of the reduction step follows a rate law. This means that the reaction rate is proportional to the product of the concentrations of the reactants, each concentration raised to a coefficient (Fogler, 2004). Therefore, we write the rate r_r for the reaction between $AuCl_4^-$ and CtH_2^- in the form:

$$r_r = k_r C_{AuCl_4^-}^l \cdot C_{CtH_2^-}^n \tag{3.3}$$

where r_r is the formation rate of gold atoms in $mol/(m^3 s)$, k_r is the reduction rate constant, and l and n are the rate orders of $AuCl_4^-$ and CtH_2^-, respectively.

While investigating the synthesis in the presence of an excess of sodium citrate, Chakraborty et al. (2016) found that Eq. (3.3) is first-order with respect to $AuCl_4^-$; that is, $l = 1$. So, we can write:

$$r_r = k_r C_{AuCl_4^-} \cdot C_{CtH_2^-}^n \tag{3.4}$$

To obtain the values of k_r and n, one needs data for r_r and the corresponding values of $C_{AuCl_4^-}$ and $C_{CtH_2^-}$. To obtain values for r_r, one requires data of the time evolution of the concentration of gold atoms present in the GNPs. Hendel et al. (2014) do not report data

of this kind, but give relevant information. In particular, for nanoparticles synthesized with different initial precursor concentrations, they correlated the amount of gold initially present in the precursor to the UV–vis absorbance at 400 nm obtained at the end of the synthesis. By doing so, they observed that such quantities are linearly related. Because all the gold in the precursor converts into nanoparticles, they concluded that the UV–vis absorbance at 400 nm is proportional to the amount of gold atoms present in the solid phase. Consequently, one can use data of the time evolution of the UV–vis absorbance at 400 nm to determine the time evolution of the concentration of gold atoms present in the solid phase. However, since the data of Hendel et al. (2014) were obtained at the end of the synthesis only, we could not use them to determine r_r (no time-resolved data are available). To this end, we instead used the data of Ji et al. (2007), who investigated the synthesis at 100 °C for a fixed initial value of precursor concentration, equal to 0.25 mol/m^3, and an initial value of the citrate-to-gold molar ratio varying between 0.7 and 28 (values referred to the synthesis solution). Ji et al. reported the time evolution of the UV–vis spectra in the wavelength band between 400 and 800 nm for three initial conditions; furthermore, for these and many more initial conditions, they reported the time evolution of the UV–vis peaks of the absorption spectra. One can obtain values for r_r by using either the entire UV–vis spectra or the values of their peaks. From the UV–vis spectra, one can determine the values of the UV–vis absorbance at 400 nm and subsequently the concentration of gold in the solid phase. Since these data are time-resolved, one can therefore determine the corresponding values of r_r. The disadvantage of this method is that the spectra are available only for three initial precursor concentrations, and so just three values for r_r can be found. Many more values are instead available for the peaks; for this reason, we used the time evolution of the UV–vis peaks.

One consideration is in order here. Note that using the values of the UV–vis peaks is possible since, when normalized, their time evolution is nearly identical to that of the normalized UV–vis absorbance at 400 nm. To demonstrate this, in Appendix D (Section D.1) of the SI we compare the time evolutions of the normalized UV–vis absorbances (at 400 nm) and peaks (the normalized values are obtained by dividing the actual values of the absorbance by the respective maximum absorbance values, which correspond to those at the end of the synthesis). As we can observe, the time evolutions are nearly identical. This implies that also the UV–vis peaks are linearly related to the concentration of gold in the solid phase. Therefore, we obtained the amount of gold atoms in the solid phase produced from the reduction step using the time evolution of the peaks. These data are reported in Fig. 2S(b) of the work of Ji et al. (2007).

We used these data in the limit $t \rightarrow 0$. This is because the gold atoms in the solid phase can form via both the reduction and growth steps, as illustrated in Fig. 2.1; However, in the limit $t \rightarrow 0$, because the growth step occurs solely in the presence of particles, only the reduction step plays a role. Thus, to obtain the values of k_r and n, we only used the data of r_r, and of the corresponding values of $C_{AuCl_4^-}$ and $C_{CtH_2^-}$, in this limit. In Appendix D (Section D.2) of the SI, we also show how to obtain from Fig. 2S (b) the value of the rate r_r in the limit $t \rightarrow 0$, which we denote as $r_{r,0}$. The values of $C_{AuCl_4^-}$ and $C_{CtH_2^-}$ for vanishingly short times, denoted as $C_{AuCl_4^-,0}$ and $C_{CtH_2^-,0}$, are those at quasi-equilibrium, which are attained in the synthesis solution when, after mixing the precursor solution with the reducing agent solution, the fast reactions involving H^+ ions have reached equilibrium but $AuCl_4^-$ has not significantly reacted. A sample calculation of how to obtain the values of $C_{AuCl_4^-,0}$ and $C_{CtH_2^-,0}$ for the citrate-to-gold molar ratio of 0.7 is given in Appendix A.

For $t \to 0$, we write Eq. (3.4) as follows:

$$r_{r,0} = k_r C_{AuCl_4^-,0} . C_{CtH_2^-,0}^n \tag{3.5}$$

This equation can be expressed equivalently as:

$$\log\left(\frac{r_{r,0}}{C_{AuCl_4^-,0}}\right) = n \log C_{CtH_2^-,0} + \log k_r \tag{3.6}$$

By plotting $\log(r_{r,0}/C_{AuCl_4^-,0})$ against $\log C_{CtH_2^-,0}$ for several initial molar ratios of citrate-to-gold, we obtain a straight line. The values of n and $\log k_r$ correspond to the slope and intercept of this line. For the data of Ji et al. (2007), Fig. 3.1 shows the plot of Eq. (3.6). Notice that to plot the values of $\log(r_{r,0}/C_{AuCl_4^-,0})$ and $\log C_{CtH_2^-,0}$ in the positive quadrant of the x-y plane, as done in Fig. 3.1, we multiplied both sides of Eq. (3.6) by -1; thus, the intercept of the line is equal to $-\log k_r$.

From Fig. 3.1, we can calculate the reaction order with respect to CtH_2^-. This is given by the slope of the curve and is equal to $n = 1.85$. The reduction rate constant at 100 °C, on the other hand, is equal to:

$$k_r = 10^{1.55} [\text{m}^3/\text{mol}]^{1.85} 1/s = 35.48 [\text{m}^3/\text{mol}]^{1.85} 1/s$$

We can thus write the reduction rate equation as:

$$r_r = k_r C_{AuCl_4^-} . C_{CtH_2^-}^{1.85} \tag{3.7}$$

3.2. Precursor passivation step

As previously discussed, the passivation step occurs when OH^- reacts with a portion of $AuCl_4^-$ to form $AuCl_3(OH)^-$, since higher hydroxylated forms of the precursor are present in negligible amounts within the pH range of interest for the synthesis, which is between 3 and 8 when the pH is measured at 25 °C (Peck et al., 1991). We write the chemical reaction as:

$$AuCl_4^- + OH^- \to AuCl_3(OH)^- + Cl^- \tag{3.8}$$
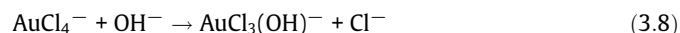
A rate equation for this step has been reported by Pacławski et al. (2012) in the form:

$$r_p = k_p C_{AuCl_4^-} . C_{OH^-} \tag{3.9}$$

where r_p is the passivation rate and k_p is the rate constant; the reaction is first-order with respect to both reactants. For the value of k_p, Pacławski et al. (2012) refer to Hanes et al. (1992), in which it is reported that $k_p = 0.0052 \text{ m}^3/(\text{mol s})$ at 16 °C.
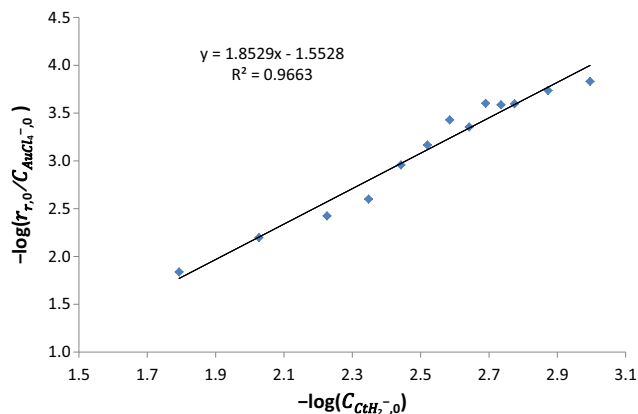
To determine the value of k_p at the standard synthesis temperature of 100 °C, we employ the experimental data of Wuithschick et al. (2015), who reported, at different temperatures, the times that $AuCl_4^-$ takes to convert significantly when hydroxylating into $AuCl_3(OH)^-$ for fixed initial concentrations of tetrachloroauric acid and NaOH in solution. These data refer to values of the mixture pH falling within the range in which the amounts of the higher hydroxylated forms of the precursor are negligible (Peck et al., 1991). Table 3.1 shows these data. From these, we can obtain the value of the activation energy of the passivation reaction.

As the initial concentrations of $HAuCl_4$ and NaOH do not change, k_p is proportional to the inverse of the reaction time τ_p, the proportionality constant, denoted as b, not depending on the reaction temperature. The reasoning for this proportionality is presented in Appendix E (Section E.1) of the SI. We can thus write:

$$k_p = \frac{b}{\tau_p} \tag{3.10}$$

Therefore, the Arrhenius equation for this step can be written as:

$$\frac{b}{\tau_p} = k_0 \exp[-E_a/RT] \tag{3.11}$$

where k_0 and E_a are the pre-exponential factor and activation energy, respectively, while T is the temperature in Kelvin and R is the universal gas constant. Rearranged, Eq. (3.11) becomes:

$$\ln\left(\frac{1}{\tau_p}\right) = \ln\left(\frac{k_0}{b}\right) - \frac{E_a}{RT} \tag{3.12}$$
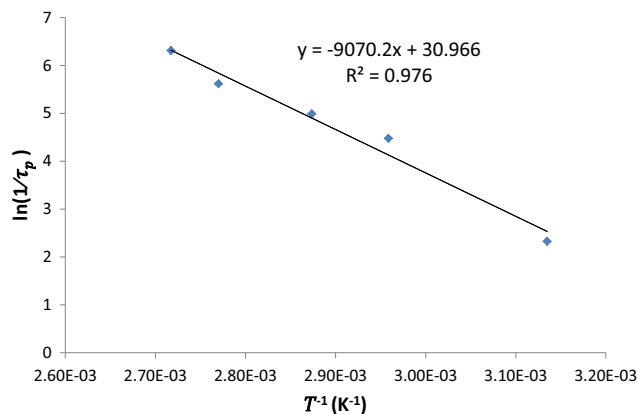
A plot of $\ln(1/\tau_p)$ versus $1/T$, based on the experimental data of Wuithschick et al. (2015), is shown in Fig. 3.2. The slope of the line is equal to -9070.2 K. Thus, we obtain:

$$E_a = 9070.2 \text{ K} \times 8.31 \text{ J/(mol K)} = 75373 \text{ J/mol}$$

Table 3.1
Characteristic time of the passivation reaction at different temperatures. The experimental data are taken from Wuithschick et al. (2015).

Temperature (°C)	Reaction time (s)
46	2150
65	250
75	150
88	80
95	40

Fig. 3.1. Plot of $y = -\log(r_{r,0}/C_{AuCl_4^-,0})$ vs $x = -\log C_{CtH_2^-,0}$ to determine the order of CtH_2^- and the kinetic constant in the reduction rate equation. The experimental data, obtained at 100 °C, are taken from Ji et al. (2007).

Fig. 3.2. Plot of $y = \ln(1/\tau_p)$ vs $x = 1/T$ to determine the activation energy of the passivation step. The experimental data, where the initial precursor concentration is constant at 0.25 mol/m³, are taken from Wuithschick et al. (2015).

Given that $k_p(16\,°C) = 0.0052$ m^3/(mol s), we can write:

0.0052 m^3/(mol s) $= k_0 \exp(-75373/(8.31 \times 289))$m^3/(mol s)

whence:

$k_0 = 2.22 \times 10^{11}$ m^3/(mol s)

Then, the Arrhenius equation for the passivation rate constant reads:

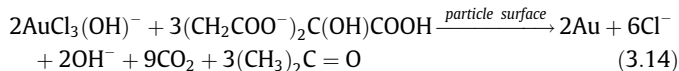$$k_p = 2.22 \times 10^{11} \exp[-75373/RT] \text{ m}^3/(\text{mol s}) \qquad (3.13)$$

Thus, at 100 °C, we have:

$$k_p(100\,°C) = 2.22 \times 10^{11} \exp[-75373/(8.31 \times 373)]$$
$$= 6.1 \text{ m}^3/(\text{mol s})$$

By an indirect method, reported in Appendix F of the SI, we obtained an estimated value of 1.9 m^3/(mol s) for k_p at 100 °C, confirming that the (more reliable) value found here is reasonable.

3.3. Seed growth step

The growth step involves a *continuous* increase of the size of the seed particles that occurs when the gold atoms produced from the reduction of $AuCl_3(OH)^-$ integrate onto the surface of the seed particles (shown in Fig. 2.1). Using molecular thermodynamic simulations, Ojea-Jimenez and Campanera (2012) reported that the reducing agent for this step is CtH^{2-}. We can therefore write the balanced chemical equation for this step as a reaction between $AuCl_3(OH)^-$ and CtH^{2-} by substituting in Eq. (3.2) $AuCl_4^-$ with $AuCl_3(OH)^- + Cl^- - OH^-$ and CtH_2^- with $CtH^{2-} + H^+$. This gives:

$$2AuCl_3(OH)^- + 3(CH_2COO^-)_2C(OH)COOH \xrightarrow{\text{particle surface}} 2Au + 6Cl^-$$
$$+ 2OH^- + 9CO_2 + 3(CH_3)_2C=O \qquad (3.14)$$

where we have explicitly indicated that this reaction occurs on the surface of the gold nanoparticles.

Eq. (3.14) is the balanced chemical equation for the growth step. Like the reduction step, its stoichiometry requires that (on the particle surface) three moles of CtH^{2-} reduce two moles of $AuCl_3(OH)^-$.

The growth model depends on the controlling mechanism. The two mechanisms are mass transfer and surface reaction (Mersmann, 2001). Here we assume that growth is controlled by the latter mechanism. This assumption is based on an analysis of the experimental data reported in Fig. 2(d) of the article of Polte et al. (2010), which presents the time evolution of the particle mean size (Fig. B.1 in Appendix B of the SI reproduces this figure). The data reveals that the growth rate is constant over a large time interval; only towards the end of the synthesis it first appears to increase slightly and then it progressively decreases, eventually vanishing. The decrease is expected and is due to the depletion of the driving force (that is, of the concentration of $AuCl_3(OH)^-$). For growth controlled by mass transfer (that is, mass transfer limited), the growth rate decreases with size (Viswanatha and Sarma, 2007). Since this behaviour is not observed experimentally, we assume that surface reaction controls particle growth. A more detailed analysis is provided in Appendix B of the SI. The same assumption was also made by Kumar et al. (2007). In deriving the growth model, we thus assume that the growth rate follows a rate law that depends on the concentrations of the reactants (that is, $AuCl_3(OH)^-$ and CtH^{2-}) and on the specific particle surface. So, we write:

$$\frac{dC_{Au}}{dt} = Ak_g C_{AuCl_3(OH)^-}^g \cdot C_{CtH^{2-}}^h \qquad (3.15)$$

where C_{Au} represents the moles of gold atoms present in the particles per unit volume of mixture; this concentration, consequently, increases only because of growth (since nucleation is absent), and so dC_{Au}/dt is directly related to the rate of change of the particle size (see Appendix B for further details). Also, in Eq. (3.15), k_g is the reaction constant, A is the particle surface area per unit volume of mixture, and g and h are the reaction orders for $AuCl_3(OH)^-$ and CtH^{2-}, respectively.

Eq. (3.15) contains three constants: k_g, g and h. We take g and h to be equal to one, following Turkevich et al. (1951), who reported the order of the two reactants in the growth process to be unity. Thus, we have:

$$\frac{dC_{Au}}{dt} = Ak_g C_{AuCl_3(OH)^-} \cdot C_{CtH^{2-}} \qquad (3.16)$$

To determine the value of k_g, we still employ the data in Fig. 2 (d) of the article of Polte et al. (2010), where the initial concentrations of the precursor and reducing agent in the synthesis solution are 0.25 mol/m^3 and 2.5 mol/m^3, respectively, and the solution temperature is 75 °C. As this figure describes the time evolution of the mean size, we can obtain the growth rate ds_m/dt from Eq. (3.16) as:

$$\frac{ds_m}{dt} = \left(\frac{m_a}{3\rho m_v}\right) k_g C_{AuCl_3(OH)^-} C_{CtH^{2-}} \qquad (3.17)$$

where m_a is the particle area shape factor (which we set equal to π, assuming that the particles are spherical), ρ is the molar density of gold, taken to be 10^5 mol/m^3 (Kumar et al., 2007), m_v is the particle volume shape factor (which we set equal to $\pi/6$, assuming that the particles are spherical) and s_m is the mean particle diameter. See Appendix B of the SI for the derivation of this equation.

As previously illustrated, the mean particle size can be affected by seed formation (caused by aggregation) and growth. In the range 20–70 min in the Fig. 2(d), the particles no longer aggregate, since the number concentration of particles is constant. However, the particle mean size increases; this can only be due to growth. At any particular time within this time interval, we can calculate the values of ds_m/dt, $C_{AuCl_3(OH)^-}$, $C_{CtH^{2-}}$ and A, and then obtain the value of k_g from Eq. (3.17). From the calculations reported in Appendix B of the SI, at 75 °C the constant k_g is equal to 2.0×10^{-6} m^4/(mol s).

To obtain the value of k_g at 100 °C, we employ additional experimental data reported by Polte et al. (2010) for the same initial concentrations of precursor and reducing agent but at two other temperatures: 85 and 100 °C. These additional data show that the time scale of the growth step, which is the time required for the particle size to change significantly due to growth, decreases from about 40 mins at 75 °C to about 23 and 15 min at 85 and 100 °C, respectively (Polte et al., 2010). From these times, we can calculate the activation energy of the growth step. Similarly to what we discussed in relation to the passivation step, we can relate the constant k_g to the inverse of the growth time scale τ_g as follows:

$$k_g = \frac{b}{\tau_g} \qquad (3.18)$$

where b is a proportionality constant. The reasoning for this equation is presented in Appendix E (Section E.2) of the SI. Then, we calculate the activation energy E_a for the growth step using the Arrhenius equation (Mersmann, 2001):

$$\frac{b}{\tau_g} = k_0 \exp[-E_a/RT] \qquad (3.19)$$

where k_0 is the pre-exponential factor for the growth step. By rearranging Eq. (3.19), we obtain:
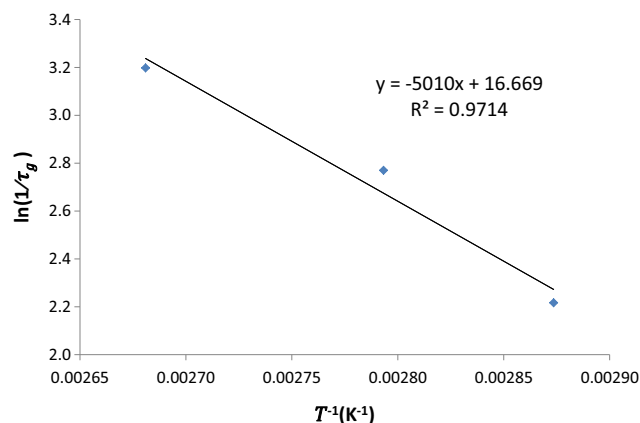
Fig. 3.3. Plot of $y = \ln(1/\tau_g)$ vs $x = 1/T$ to determine the activation energy of the growth step. The experimental data, where the initial concentrations of the precursor and reducing agent in the synthesis solution are 0.25 mol/m³ and 2.5 mol/m³, respectively, are taken from Polte et al. (2010).

$$\ln\left(\frac{1}{\tau_g}\right) = \ln\left(\frac{k_0}{b}\right) - \frac{E_a}{RT} \tag{3.20}$$

Fig. 3.3 shows the plot of $\ln(1/\tau_g)$ versus $1/T$, based on the experimental data of Polte et al. (2010). The value of the slope is -6102.6 K. From this value:

$$E_a = 5010 \text{ K} \times 8.31 \text{ J/(mol K)} = 41633 \text{ J/mol}$$

Given that $k_g(75\,^\circ\text{C}) = 2.00 \times 10^{-6}$ m⁴/(mol s), we can write:

$$2.00 \times 10^{-6} \text{ m}^4/(\text{mol s}) = k_0 \exp(-41633/(8.31 \times 348)) \text{ m}^4/(\text{mol s})$$

whence:

$$k_0 = 3.58 \text{ m}^4/(\text{mol s})$$

and the value of k_g at 100 °C is:

$$k_g(100\,^\circ\text{C}) = 3.58 \text{ m}^4/(\text{mol s}) \exp[-41633/(8.31 \times 373)]$$
$$= 5.25 \times 10^{-6} \text{ m}^4/(\text{mol s})$$

3.4. Seed formation step

The seed-mediated mechanism requires that the gold atoms, formed from the reduction step, aggregate into equal-sized "seed particles". If the number concentration of gold atoms produced from the reduction step were approximately equal to the final number concentration of gold nanoparticles, each gold atom would coincide with a seed particle, which would then "grow" into a final GNP (note that in this case the term "grow" is incorrect, since, at least initially, the particles are made up of few gold atoms; growth is possible solely when the particles comprise several atoms, so that the rate of change of their size caused by the attachment of additional atoms can be regarded as a continuous process). This is a limiting case for the seed particle size, not expected to be observed experimentally. The number concentration of gold atoms is expected to be far greater than the number concentration of the final GNPs, the seed size being consequently larger than the size of a gold atom, which is 0.272 nm (Cordero et al., 2008). In this section, we propose a method for calculating the diameter of the seed particles; however, due to its complexity, we do not attempt to model the aggregation process or to determine its kinetics.

Because no further aggregation occurs after the seed formation step, the number concentration of the seed particles must be equal

to the final number concentration of GNPs (Wuithschick et al., 2015). Assuming complete conversion of the precursor into GNPs and a monodisperse particle size distribution, we can estimate the final number concentration of GNPs as follows:

$$\frac{C_{HAuCl_4}}{\rho m_v s_f^3} \tag{3.21}$$

where C_{HAuCl_4} is the initial concentration of the precursor in the synthesis solution, and s_f is the final mean particle diameter.

The number concentration of seed particles, however, can also be calculated using the following equation:

$$\frac{C_s}{\rho m_v s_s^3} \tag{3.22}$$

where C_s is the amount of precursor that forms the seed particles per volume of synthesis solution and s_s is the seed diameter.

The value of C_{HAuCl_4} is known. To determine the value of C_s, we use the selectivity of the reduction step over the passivation step, defined as the ratio of the amount of precursor that forms gold atoms in the reduction step to the amount of precursor that becomes passivated. The amount of precursor that forms gold atoms and then seed particles is equal to VC_s and can be expressed as:

$$VC_s = V \int_0^{t_s} r_r dt \tag{3.23}$$

where V is the volume of synthesis solution, r_r is the reaction rate for the reduction step, t is the time, and t_s is the total synthesis time.

Similarly, the amount of precursor that becomes passivated can be expressed as:

$$V(C_{HAuCl_4} - C_s) = V \int_0^{t_s} r_p dt \tag{3.24}$$

where r_p is the rate of the passivation reaction. The selectivity S is defined as follows:

$$S = \frac{\displaystyle\int_0^{t_s} r_r dt}{\displaystyle\int_0^{t_s} r_p dt} \tag{3.25}$$

Using Eqs. (3.7) and (3.9), we thus have:

$$S = \frac{k_r \displaystyle\int_0^{t_s} [C_{AuCl_4^-}] \cdot [C_{CtH_2^-}]^{1.85} dt}{k_p \displaystyle\int_0^{t_s} [C_{AuCl_4^-}][C_{OH^-}] dt} \tag{3.26}$$

To use this equation to obtain S, we need to know the time profiles of $C_{AuCl_4^-}$, $C_{CtH_2^-}$ and C_{OH^-}. For synthesis conditions where the molar ratio of initial concentrations of sodium citrate to tetra-chloroauric acid in the synthesis solution is equal to or greater than five, we assume that the values of $C_{CtH_2^-}$ and C_{OH^-} do not change significantly from their values at quasi-equilibrium, denoted as $C_{CtH_2^-,0}$ and $C_{OH^-,0}$, respectively. The reasoning is discussed in Appendix C of the SI. Thus, we can write:

$$S = \frac{k_r}{k_p} \frac{[C_{CtH_2^-,0}]^{1.85}}{[C_{OH^-,0}]} \frac{\displaystyle\int_0^{t_s} [C_{AuCl_4^-}] dt}{\displaystyle\int_0^{t_s} [C_{AuCl_4^-}] dt} = \frac{k_r}{k_p} \frac{[C_{CtH_2^-,0}]^{1.85}}{[C_{OH^-,0}]} \tag{3.27}$$

Writing a material balance equation over Au in the precursor, we have:

$$C_{HAuCl_4} = C_s + C_s/S \tag{3.28}$$

where C_s/S is the amount of precursor that becomes passivated. Solving Eq. (3.28) for C_s, substituting the resulting expression of

C_s into Eq. (3.22) and then equating the quantity obtained to that reported in Eq. (3.21) yields:

$$s_s = s_f \left(\frac{S}{1+S} \right)^{1/3} \tag{3.29}$$

Note that the relation above applies to synthesis conditions where the molar ratios of the initial concentration of sodium citrate to tetrachloroauric acid in the synthesis solution are equal to or greater than five. As $S \rightarrow 0$, this limit being approached at high pH, $s_s \rightarrow 0$; before reaching this extreme case, s_s will become equal to the size of a gold atom, as previously discussed.

Based on the criterion above, we simplify the balanced chemical equations for the reduction, passivation and growth steps, and present a model for the citrate synthesis method as follows.

3.5. Nanoparticle synthesis model

The proposed model is based on the seed-mediated mechanistic description of the synthesis describing how the gold nanoparticles evolve as they form. To simplify the kinetic equations, we restrict to initial molar ratios of citrate to gold to values equal to or greater than five. For this condition, as shown in Fig. C.2 in Appendix C of the SI, the pH value at quasi-equilibrium is approximately equal to that at the end of the synthesis. This assumption has many implications. First, because the concentration of H^+ ions determines the pH, this concentration and that of OH^- ions do not change from their values at quasi-equilibrium. Second, the relative mole fractions among the four citrate species also do not change from the values present at quasi-equilibrium, even though the sum of their amounts decreases owing to the reduction reactions of CtH_2^- and CtH^{2-} with $AuCl_4^-$ and $AuCl_3(OH)^-$, respectively. This second implication is illustrated in Fig. C.1 in Appendix C of the SI, where specifying the pH value of the reaction solution determines the relative mole fractions among the four citrate species. Here, to illustrate why, we consider the equilibrium equations for citrate speciation reactions in Eqs. (2.4)–(2.6), which take place nearly instantly at a time scale of $\sim 10^{-11}$ s (Pines et al., 1997). For reaction (2.4), the equilibrium equation can be written as:

$$\frac{K_{R3}}{C_{H^+}} = \frac{C_{Ct^{3-}}}{C_{CtH^{2-}}} \tag{3.30}$$

Being an equilibrium constant, K_{R3} assumes a constant value which depends on the synthesis temperature. At a fixed synthesis temperature and once the pH value of the synthesis solution is determined at quasi-equilibrium, the ratio of $C_{Ct^{3-}}/C_{CtH^{2-}}$ in Eq. (3.30) assumes a constant value. Analogously, for Eqs. (2.5) and (2.6), the ratios of $C_{CtH^{2-}}/C_{CtH_2^-}$ and $C_{CtH_2^-}/C_{CtH_3}$ are constant while the synthesis progresses, if one assumes that the mixture pH remains constant at the quasi-equilibrium value.

This assumption also implies that we cannot write the chemical equations in terms of the real reactants and products involved in the reduction, passivation and growth steps. For example, by keeping the concentration of OH^- constant, we cannot write that OH^- reacts with $AuCl_4^-$ to generate $AuCl_3(OH)^-$. We have to write instead that OH^- acts "as a catalyst", converting the precursor to another form, not available to produce the gold atoms in the seed particles, but available to grow them. In reality, since OH^- is consumed by the passivation step, this reaction shifts the equilibrium reaction in Eq. (2.1) to the right, so as to keep the concentration of OH^- constant. In the process, Eq. (2.1) yields an additional amount of H^+. This additional amount then shifts the speciation reactions of citrate in Eqs. (2.2)–(2.4) to the right. To develop a model that accounts for the real reactants and products, apart from the reaction rates so far considered, we need to know also the rates of the reactions involving H^+. We do not know these rates, but we know that they are extremely large. Accordingly, we use the quasi-equilibrium approximation instead. In doing so, we could still consider all the reactants and products, but we would have to solve the quasi-equilibrium at every time step of the simulation, which is too demanding. To avoid doing this, we opt for a simplified model that nevertheless is able to correctly predict the evolution of the particle size, ensuring that the amount of gold initially present in the precursor eventually turns into nanoparticles. As for the reactants, this simplified model cannot consider all the products of the reactions. Rather, it lumps a number of them into fictitious components.

3.5.1. Chemical reactions

For the reaction in Eqs. (3.2), we rewrite the chemical reaction as:

$$2T + 3(x \cdot Ct) \rightarrow 2Au + Pr1 \tag{3.31}$$

T represents the gold in $AuCl_4^-$, Ct represents the sum of all the species of citrate, x represents the relative mole fraction (among the four citrate species) of CtH_2^- at the quasi-equilibrium pH, Au represents the gold in the GNPs, and $Pr1$ represents all by-products from the reduction step, lumped together.

For the reaction in Eq. (3.8), we have:

$$T \xrightarrow{B} K \tag{3.32}$$

B represents OH^-, which is assumed to have a constant concentration, and acts as a catalyst; K represents the gold that becomes passive and that eventually grows the seed particles.

For the reaction in Eq. (3.14), we have:

$$2K + 3(y \cdot Ct) \xrightarrow{Particles} 2Au + Pr2 \tag{3.33}$$
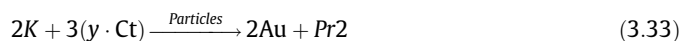
y denotes the relative mole fraction of CtH^{2-} at the quasi-equilibrium pH, whilst $Pr2$ represents all by-products from the surface reduction, lumped together.

3.5.2. Mole balances

Assuming that the reaction solution is perfectly mixed (which implies that all intensive properties, such as temperature and concentrations, are uniform), we can select as control volume the region (of constant volume V) occupied by the mixture contained in the batch reactor wherein the synthesis takes place. The balance equations of the mixture components are then those reported below.

3.5.2.1. Precursor. This is consumed by both the reduction and passivation steps. Considering Eqs. (3.7) and (3.9), the material balance equation takes the form:

$$\frac{dC_T}{dt} = -k_r C_T (x C_{Ct})^{1.85} - k_p C_T C_B \tag{3.34}$$

3.5.2.2. Total citrate species. At any time, we consider the sum of the concentrations of all the citrate species (i.e., Ct^{3-}, CtH^{2-}, CtH_2^- and CtH_3), which we denote as C_{Ct}, and model the time variation of this total concentration caused by the reduction and growth reactions. The reduction step consumes CtH_2^-, whose amount, at any time, is given by xC_{Ct}, whilst the growth step consumes CtH^{2-}, whose amount, at any time, is given by yC_{Ct}. Considering the stoichiometric ratios in Eqs. (3.2) and (3.14) and the growth rate equation in Eq. (3.16), the material balance equation on the total citrate species is:

$$\frac{dC_{Ct}}{dt} = -(3/2)k_r C_T (x C_{Ct})^{1.85} - (3/2)m_a k_g C_K (y C_{Ct}) \int_{s_s}^{\infty} s^2 f(s,t) ds \tag{3.35}$$

3.5.2.3. Hydroxyl ions. Having assumed that the pH of the mixture is constant at the quasi-equilibrium value, we simply write that the concentration of hydroxyl ions is constant:

$$C_B = constant \tag{3.36}$$

3.5.2.4. Passive precursor. The precursor passive form is generated by the passivation step and consumed by the growth step. Considering Eqs. (3.8) and (3.16), the material balance equation reads:

$$\frac{dC_K}{dt} = k_p C_T C_B - m_a k_g C_K (yC_{Ct}) \int_{s_s}^{\infty} s^2 f(s,t) ds \tag{3.37}$$

3.5.2.5. By-products. The reduction and growth reactions generate by-products such as CO_2, $(CH_3)_2C = O$ and Cl^-, as shown in Eqs. (3.2) and (3.14). To ensure that total mass is conserved, we report the balance equations for these other by-products. To account for those generated in the reduction step, lumped into $Pr1$, we write:

$$\frac{dC_{Pr1}}{dt} = (1/2)k_r C_T (xC_{Ct})^{1.85} \tag{3.38}$$

To account for the by-products generated in the growth step, lumped in $Pr2$, we write the following material balance equation:

$$\frac{dC_{Pr2}}{dt} = (1/2)m_a k_g C_K (yC_{Ct}) \int_{s_s}^{\infty} s^2 f(s,t) ds \tag{3.39}$$

3.5.2.6. Gold nanoparticles. In writing a continuity statement for the particle phase, one employs the population balance modelling approach (Ramkrishna, 2000; Marchisio and Fox, 2013). This is based on the size distribution of the particles (PSD) and accounts for the processes that affect the particle population. In modelling the evolution of the GNPs, we do not model the nucleation process, and the subsequent aggregation process that yields the seed particles. Instead, we consider a nucleation term that accounts directly for the "nucleation" of the seed particles, whose size is determined using the method specified in Section 3.4. After the seed particles have "nucleated", they grow into the final GNPs. In the previous model by Kumar et al. (2007), the authors employed this modelling approach to describe the evolution of the GNPs by nucleation and growth, assuming that the nucleus had a known diameter of 2 nm. However, as illustrated in Section 3.4, the seed diameter does not have a constant value; this depends on the synthesis conditions.

As we have assumed that the reaction system is uniform, the PSD does not depend on the real-space coordinates. The PSD, which we denote as $f(s,t)$, depends solely on the particle size and on the time coordinate. By definition, $f(s,t)ds$ represents the number of particles per unit volume of synthesis solution with size in the differential range ds about the size s at time t. For details about the derivation of the population balance equation, we refer to Ramkrishna (2000) and Marchisio and Fox (2013). The equation in our case reads:

$$\partial_t f(s,t) = -\partial_s [f(s,t).G_s] + \left(\frac{1}{\rho m_v s_s^3}\right) k_r C_T (xC_{Ct})^{1.85} \delta(s - s_s) \tag{3.40}$$

where

$$G_s = \left(\frac{m_a}{3\rho m_v}\right) k_g C_K (yC_{Ct}) \tag{3.41}$$

Here G_s is the particle growth rate, previously reported in Eq. (3.17).

The term on the left-hand side of Eq. (3.40) represents accumulation, while the first term on the right-hand side accounts for the growth process due to surface reaction. The second and last term on the right-hand side accounts for the formation of the seed particles. In this term, $k_r C_T (xC_{Ct})^{1.85}$ gives the rate of formation of gold

atoms in mol/(m³ s) which forms seed particles, and $\delta(s - s_s)$ indicates that all the seed particles have equal diameter s_s, given by Eq. (3.29). The term $\rho m_v s_s^3$ is the moles of gold present in one seed particle. We have assumed here that as soon as the gold atoms form, they immediately aggregate, turning into seed particles; we made this assumption, because, for the time being, we do not know the aggregation rate and do not have a model for the aggregation process. Developing one is quite complex, and doing so is part of future work.

4. Results and discussion

To solve the model, we used the numerical code Parsival, which is commercially available for solving population balance equations. For the computational details of this software, we refer the reader to Wulkow et al. (2001). In this code, the equations are solved on a mass basis; therefore, we transformed the equations, which were derived on a mole basis, into a mass basis. Since the reaction system is uniform, we converted the mole into kg by writing:

$$m_i = C_i Y_i V \tag{4.1}$$

where m is the mass in kg, C is the concentration in mol/m^3, Y is the molar mass of species i in kg/mol and V is the volume of the synthesis solution. By differentiating Eq. (4.1) with respect to the time, one obtains:

$$\frac{dm_i}{dt} = Y_i V \frac{dC_i}{dt} + C_i Y_i \frac{dV}{dt} \tag{4.2}$$

In the synthesis, the reaction mixture is dilute, containing predominantly water. One can therefore assume that the volume of the mixture is constant. Therefore, Eq. (4.2) reduces to:

$$\frac{dm_i}{dt} = Y_i V \frac{dC_i}{dt} \tag{4.3}$$

The balance equations of the model can then be expressed as follows:

$$T: \frac{d[C_T Y_T V]}{dt} = [-k_r C_T (xC_{Ct})^{1.85} - k_p C_T C_B]Y_T V \tag{4.4}$$

$$Ct: \frac{d[C_{Ct} Y_{Ct} V]}{dt} = -1.5[k_r C_T (xC_{Ct})^{1.85} + m_a k_g C_K (yC_{Ct}) \int_{s_s}^{\infty} s^2 f(s,t) ds]Y_{Ct} V \tag{4.5}$$

$$Pr1: \frac{d[C_{Pr1} Y_{Pr1} V]}{dt} = [0.5 \cdot k_r C_T (xC_{Ct})^{1.85}]Y_{Pr1} V \tag{4.6}$$

$$K: \frac{d[C_K Y_K V]}{dt} = [k_p C_T C_B - m_a k_g C_K (yC_{Ct}) \int_{s_s}^{\infty} s^2 f(s,t) ds]Y_K V \tag{4.7}$$

$$Pr2: \frac{d[C_{Pr2} Y_{Pr2} V]}{dt} = [0.5 \cdot m_a k_g C_K (yC_{Ct}) \int_{s_s}^{\infty} s^2 f(s,t) ds]Y_{Pr2} V \tag{4.8}$$

On the other hand, the population balance equation in Eq. (3.40) expresses how the particle size distribution evolves under the influence of the formation and growth of the seed particles. These are assumed to be formed at the seed size s_s, represented by the Dirac delta function. Because this function cannot be implemented in Parsival, we employed a similar but smooth function: a Gaussian distribution with mean equal to s_s (i.e., the size of the seed particles) and an extremely small standard deviation. In Agunloye et al. (2017), we showed that assuming a narrow Gaussian distribution does not affect the final results. For reaction conditions in which the initial

values of the citrate-to-gold molar ratio are equal to or greater than five, we followed the methodology presented in Section 3.4 to determine the values of x and y, which are the relative mole fractions of CtH_2^- and CtH^{2-}, respectively.

The values of the constants k_r, k_p and k_g also need to be specified. At 100 °C, their values, as reported in Section 3, are:

$$k_r = 34.48[m^3/mol]^{1.85}1/s; \quad k_p = 6.1 \ m^3/(mol \ s);$$

$$k_g = 5.25 \times 10^{-6} \ m^4/(mol \ s)$$

Finally, in solving model equations in the synthesis model, we had to specify the initial conditions and the value of s_s. These initial conditions must satisfy the criterion that the initial value of the citrate-to-gold molar ratio in the synthesis solution be equal to or greater than five at a temperature of 100 °C. In the literature, researchers such as Turkevich et al. (1951), Ji et al. (2007), Zabetakis et al. (2012) and Wuithschick et al. (2015) used experimental conditions that satisfy this condition. Albeit most of the experimental data reported by Turkevich et al. were for molar ratios below five, the authors reported a final mean size of 20 nm at an initial value of the citrate-to-gold molar ratio of 7.6, which can be regarded as the synthesis standard condition. Similarly, Zabetakis et al. investigated the synthesis at a single initial molar ratio of five. However, while keeping the molar ratio constant, they altered the initial pH of the precursor by changing the initial concentrations. Ji et al. and Wuithschick et al., on the other hand, investigated the synthesis at several initial molar ratios at or greater than five.

The value of the seed size s_s can be calculated employing Eq. (3.29). In the following section, we validate the predictions obtained from this equation using the synthesis conditions of Wuithschick et al. (2015), where the size of the seeds is reported. Once Eq. (3.29) has been validated, we use it to illustrate that the value of the seed size is not constant, but depends on the initial conditions of the synthesis.

4.1. Seed size validation and sensitivity analysis

To validate the value of the seed diameter obtained from Eq. (3.29), we employ the standard condition in the work of Wuithschick et al. (2015), where the molar ratio of citrate-to-gold is ten, the initial precursor concentration in the synthesis solution at 100 °C is 0.25 mol/m³, and the final particle mean diameter is 18.6 nm. In this condition, the authors reported a value of the seed diameter of ∼ 3 nm. This value allows validating the predictions of Eq. (3.29).

To obtain the value of S, we use Eq. (3.27). At 100 °C, $k_r = 35.48[m^3/mol]^{1.85}1/s$ and $k_p = 6.1 \ m^3/(mol \ s)$. To determine the values of $C_{CtH_2^-,0}$ and $C_{OH^-,0}$, we follow the procedure described in Appendix A of the SI; these are $1.4 \times 10^{-3} \ mol/m^3$ and $7.44 \times 10^{-3} \ mol/m^3$, respectively, while the pH value is 6.06. Thus:

$$S = \frac{k_r}{k_p} \frac{[C_{CtH_2^-,0}]^{1.85}}{[C_{OH^-,0}]} = 4.11 \times 10^{-3}; \quad s_s = s_f \left(\frac{S}{1+S}\right)^{1/3} = 2.97 \ nm$$

This value agrees with the measured seed size (∼ 3 nm) measured by Wuithschick et al. (2015). We can therefore specify this value in the numerical code to implement the synthesis model for the standard condition of Wuithschick et al. (2015). Notice that

changing the value of s_s, given the same synthesis conditions, does affect the model predictions. This indicates that the model is sensitive to the value assigned to the size of the seeds, and this value, therefore, has to be properly estimated. To illustrate this point, we changed the value of 2.97 nm by ±1%, ±10% and ±50% and then solved the model numerically using these new, incorrect values of the seed diameter. Table 4.1 shows the results.

These results reveal that as the seed diameter increases from the actual size of 2.97 nm, the final mean diameter increases. Because the selectivity is determined by the initial reaction conditions, the amount of the precursor that forms the seed particles is fixed. Increasing the seed size, therefore, decreases the number density of seeds. These seeds then grow into final GNPs with a mean diameter larger than 18.8 nm. Hence, specifying the accurate value of the seed diameter in the model is important to predict correctly the final mean diameter of the NPs.

In the calculations above, the model used as input the final size of the NPs, its output being the size of the seeds, which we were able to validate using the experimental information provided by Wuithschick et al. (2015). Nevertheless, one would like the model to be fully predictive and have as output also the final NP size. To this end, we need a submodel or an empirical correlation that can predict the seed size once the initial synthesis conditions are selected. Developing a submodel based on theoretical arguments is quite challenging and we regard it as part of future work. To render the model fully predictive, we opt for a correlation.

4.2. Seed size correlation

To derive a correlation able to predict the size of the seeds, we employ Eq. (3.29) to calculate the seed size for some syntheses for which experimental data are available and then relate the values obtained to the initial conditions adopted in the syntheses. We employ the experimental data of Ji et al. (2007), whose initial conditions satisfy the criterion for the synthesis model (i.e., the initial citrate-to-gold molar ratio must be equal to or greater than five). Ji et al. (2007) investigated the synthesis at 100 °C *for a fixed initial value of precursor concentration*, equal to 0.25 mol/m³, and an initial value of the citrate-to-gold molar ratio varying between 0.7 and 28 (values referred to the synthesis solution). To derive the correlation, we considered the syntheses in which the initial values of the citrate-to-gold molar ratio were 5.6, 7.7, 8.4, 14 and 27.8, whilst the final mean sizes of the GNPs were 19.79, 25.23, 25.87, 31.01, and 30.58 nm, respectively. From the initial conditions of these five syntheses and following the procedure described in Section 4.1, we could calculate the corresponding values of the selectivity S. Then, we calculated the seed diameters from Eq. (3.29). Fig. 4.1A shows how the seed diameter varies with the initial value of the citrate-to-gold molar ratio.

The figure shows that the seed size varies linearly with the citrate-to-gold molar ratio when the initial precursor concentration and temperature are constant (at 0.25 and 100 °C, respectively). Once the initial conditions of the synthesis are assigned, the value of the quasi-equilibrium pH can be calculated using the method outlined in Appendix A of the SI. Once the value of the quasi-equilibrium pH is known for each value of the initial citrate-to-gold molar ratio, Fig. 4.1B can be generated. This expresses the final mean diameter of the NPs as a function of the quasi-equilibrium pH. Also in this case the functional relation is

Table 4.1

Sensitivity analysis of the model predictions (in terms of GNP final mean diameter) on the seed diameter. The value of the citrate-to-gold molar ratio is ten.

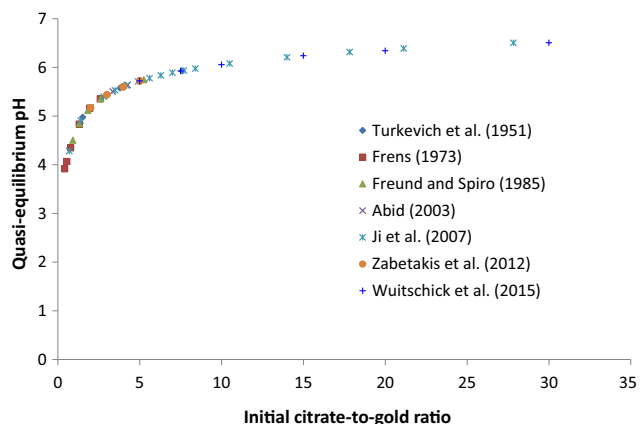| Deviation from the actual seed size	−50%	−10%	−1%	0%	1%	10%	50%
Seed diameter (nm)	1.49	2.67	2.94	2.97	3.00	3.27	4.46
Final NP diameter (nm)	10.30	17.30	18.40	18.80	19.30	20.90	28.20
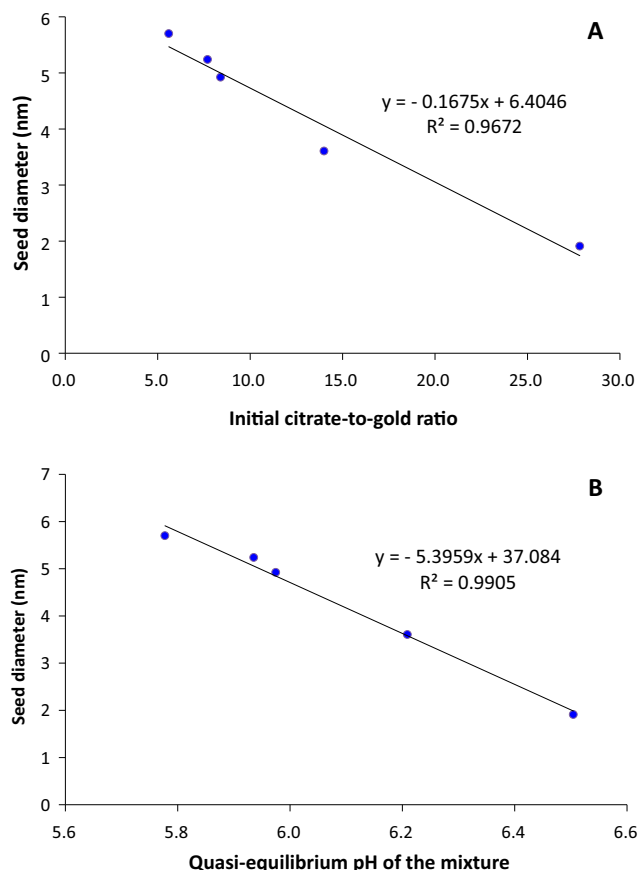
Fig. 4.1. (A) Seed diameter predicted by Eq. (3.29) as a function of the initial value of the citrate-to-gold molar ratio. (B) Seed diameter predicted by Eq. (3.29) as a function of the quasi-equilibrium pH. The values refer to the syntheses studied experimentally by Ji et al. (2007) at 100 °C. The initial concentration of gold in the synthesis solution is equal to 0.25 mol/m³ in all cases.

linear, the correlation fitting the data even better than in Fig. 4.1A. Thus, letting pH_Q denote the quasi-equilibrium pH, we can write:

$$s_s = A \cdot pH_Q + B \tag{4.9}$$

where $A = -5.40$ and $B = 37.08$ nm.

Notice that the quasi-equilibrium pH depends solely on the citrate-to-gold molar ratio, being independent of the initial precursor concentration. We verified this using the thermodynamic model presented in Appendix A of the SI. We employed this model also to generate Fig. 4.2, in which we report the values of the quasi-equilibrium pH against those of the citrate-to-gold molar ratio for syntheses investigated experimentally by various research groups. These syntheses had different initial values of precursor concentration, but, as the figure reveals, the experimental points fall on one curve; this implies that the only variable that affects the quasi-equilibrium pH is indeed the citrate-to-gold molar ratio.

The correlation (4.9) is valid at a temperature of 100 °C for a fixed value of precursor concentration. We now extend its range of validity by considering experimental data referring to syntheses in which this concentration varies, while *the value of the initial citrate-to-gold molar ratio is kept fixed*. To this end, we employ the synthesis conditions of Zabetakis et al. (2012), who kept the molar ratio equal to 5 whilst considering the precursor concentrations $C_{T0} = 0.3, 0.6, 1.0, 1.2,$ and 2.0 mol/m³ in the synthesis solution. We use three out of these five initial conditions to obtain the dependence on the initial precursor concentration, while we use the remaining two in Section 4.3 to test the model predictions. These three initial conditions are $C_{T0} = 0.3, 1.0,$ and 2.0 mol/m³, which yielded GNPs with mean sizes of 18.70, 14.40, and 16.00 nm, respectively. For these three initial conditions, we can calculate the selectivity S using the procedure in Section 4.1. Then, we calculate the seed diameter from Eq. (3.29). Fig. 4.3 shows how the seed size varies with the initial precursor concentration. From this figure, the seed diameter linearly correlates with the initial concentration of precursor. To account for the dependence of the seed size on the initial precursor concentration in Eq. (4.9), we write:
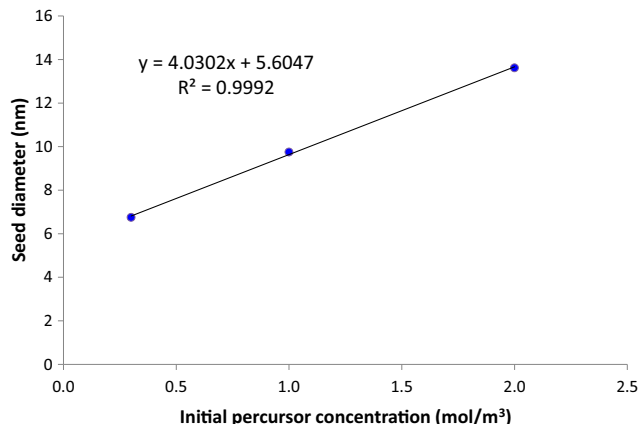
$$s_s = A \cdot pH_Q + D \cdot C_{T0} + Q \tag{4.10}$$

where $D = 4.03$ and Q is a constant.

Based on these figures, we take the values of A and D to be equal to -5.40 and 4.03, respectively. To obtain the value of Q, we equate the right-hand side of Eq. (4.10) to the right-hand side of the linear correlation equation in Fig. 4.1B, where the initial precursor concentration is 0.25 mol/m³, thus writing:

$$4.03 \cdot C_{T0} + Q = 37.08 \tag{4.11}$$

This yields $Q = 36.08$ nm. Alternatively, one could equate the right-hand side of Eq. (4.10) to the right-hand side of the linear correlation equation in Fig. 4.3, where the quasi-equilibrium pH is 5.72. This yields, $Q = 36.49$ nm. This and the previous values are quite close; they would have been identical if the correlation

Fig. 4.2. Relationship between the quasi-equilibrium pH and the initial value of the citrate-to-gold molar ratio. The data refer to syntheses conducted at 100 °C by various research groups (Turkevich et al., 1951; Frens, 1973; Freund and Spiro, 1985; Abid, 2003; Ji et al., 2007; Zabetakis et al., 2012; Wuithschick et al., 2015).

Fig. 4.3. Seed diameter predicted by Eq. (3.29) as a function of the initial precursor concentration. The values refer to the syntheses studied experimentally by Zabetakis et al. (2012) at 100 °C. The initial citrate-to-gold molar ratio in the synthesis solution is equal to five in all cases.

coefficients in Figs. 4.1B and 4.3 had been unity. As Fig. 4.1B contains more data points than Fig. 4.3, we opt for $Q = 36.08$ nm. Thus, we write Eq. (4.10) as:

$$s_s = -5.40 \cdot pH_Q + 4.03 \cdot C_{T0} + 36.08 \qquad (4.12)$$

With this correlation for the seed diameter applicable at the synthesis temperature of 100 °C, the synthesis model is fully predictive. We test the model predictions in the following section.

4.3. Model validation

In this section, we test the model by comparing its predictions against experimental data. These data refer to syntheses whose initial conditions satisfy the criterion on which the model is based, namely that the initial citrate-to-gold molar ratio must be equal to or greater than five; furthermore, they refer to syntheses conducted at a temperature of 100 °C. Three data sets are taken from the work of Ji et al. (2007) and two from the work of Zabetakis et al. (2012). Ji et al. kept the initial precursor concentration constant at $0.25 \, \text{mol/m}^3$ and varied the citrate-to-gold molar ratio considering the values of 7.0, 10.5 and 17.8. Zabetakis et al., conversely, kept the initial citrate-to-gold molar ratio constant at five and varied the initial precursor concentration, considering the values of 0.6 and $1.2 \, \text{mol/m}^3$. From these initial conditions, following the procedure outlined in Appendix A of the SI, we obtained the value of the quasi-equilibrium pH, and then calculated the corresponding values of seed diameter using Eq. (4.12). Notice that these data were not part of the data set employed to derive the seed size correlation in the previous section.
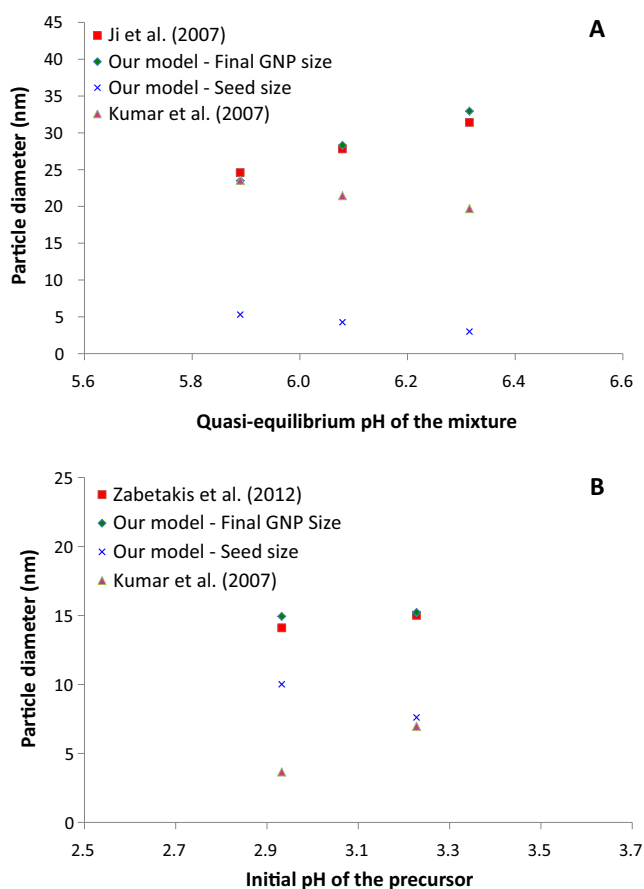

Fig. 4.4. Final particle size predicted by our model and that of Kumar et al. (2007) against the experimental data obtained by Ji et al. (A) and Zabetakis et al. (B).

For the data of Ji et al. (2007), Fig. 4.4A shows the particle sizes predicted by our model and by that of Kumar et al. (2007) against the experimental data. As shown, the predictions of our model are in very good agreement and follow the same trend as the experimental data. The values of the seed diameter calculated from Eq. (4.12) for the citrate-to-gold molar ratios of 7.0, 10.5 and 17.8 are 5.28, 4.26, and 2.99 nm, respectively. These values, also shown in Fig. 4.4A, compare reasonably well with those of 5.63, 4.25, and 2.91 nm, calculated from Eq. (3.29). These good predictions of the seed diameter explain why the model yields good predictions in terms of final particle size. As the quasi-equilibrium pH increases, indicating an increasing amount of OH⁻, the amount of precursor that generates $AuCl_3(OH)^-$ increases, while the amount of precursor that forms gold atoms and then seed particles decreases. The latter trend is confirmed by the decreasing values of the seed diameter. Thereafter, the remaining precursor, in the form $AuCl_3(OH)^-$, grows the seed particles into the final GNPs. Since the initial precursor concentration in these three initial conditions was kept constant at $0.25 \, \text{mol/m}^3$, the increasing amounts of $AuCl_3(OH)^-$ grow the seed particles to larger final sizes.

In Fig. 4.4A, we also report the values predicted by the model developed by Kumar et al. (2007). To obtain these values, we implemented and solved their model numerically. In this model, Kumar et al. assumed the seed diameter to be constant at 2 nm for different reaction conditions. The description of how their model was solved numerically, and the checks carried out to verify that the implementation is correct, are discussed in Agunloye et al. (2017). We see that the predictions from their model show an opposite trend: the predicted mean diameter decreases with increasing quasi-equilibrium pH; moreover, the model predictions are less accurate for two of the three conditions reported in Fig. 4.4A. Their model is based on a mechanistic description which is completely different from that informed by the chemistry of precursor and reducing agent in the synthesis solution; accordingly, it does not account for the important role played by the pH in this synthesis method. The pH determines the relative mole fractions of the citrate species and the quantities of precursor that reduces to gold atoms and passivates into the hydroxylated form which is able to grow the seeds $(AuCl_3(OH)^-)$. The concentration of gold atoms along with the balance of forces of attraction and repulsion determines the seed size. As discussed, this is not constant, contrary to the assumption used in the model of Kumar et al.

For the data of Zabetakis et al. (2012), Fig. 4.4B shows the values of the final particle sizes predicted by our model and by that of Kumar et al. (2007) against the experimental data. Again, the predictions of our model are in very good agreement with the latter. The values of the seed diameter in this case are larger than those reported in Fig. 4.4A for the syntheses of Ji et al. This is because the seeds are formed via an aggregation process, whose effect decreases as the value of the pH of the mixture at quasi-equilibrium conditions increases. For both syntheses conducted by Zabetakis et al. the pH value is 5.72 (the value does not change because in both syntheses the value of the citrate-to-gold molar ratio is the same). This value is lower than all the pH values characterizing the syntheses conducted by Ji et al., as one can see from Fig. 4.4A. Even if the quasi-equilibrium pH, which determines the selectivity, is identical for both conditions in Fig. 4.4B, the initial precursor concentrations are different. The larger initial concentration of precursor increases the concentration of gold atoms. These atoms aggregate more significantly to produce larger seeds, and also a greater number concentration of seed particles. As shown in Fig. 4.4B, the seed size for $C_{T0} = 1.2 \, \text{mol/m}^3$ is 10.03 nm while for $C_{T0} = 0.6 \, \text{mol/m}^3$ is 7.61 nm. For the number concentration of seed particles, obtained by solving the synthesis model, $C_{T0} = 1.2 \, \text{mol/m}^3$ yields about twice the value for $C_{T0} = 0.6 \, \text{mol/m}^3$. For the growth process, although a

larger amount of AuCl$_3$(OH)$^-$ is generated in the case of $C_{T0} = 1.2$ mol/m^3, this amount grows the greater number of seed particles (per unit volume) to almost the same final size as in the case of $C_{T0} = 0.6$ mol/m^3, as shown.

The predictions of the model by Kumar et al. (2007) deviate considerably from the experimental data, the NP final sizes being smaller than the size of the seeds yielded by our model. We have discussed in our previous work (Agunloye et al., 2017) why their model does not yield accurate predictions, and so here we do not comment on this at length. Although the model accounts for the reduction of the precursor, it does not account for the hydroxylation of the tetrachloroauric ions, a reaction that occurs in parallel with the reduction step when the precursor and reducing agent solutions are mixed.

In our model, the three most important synthesis parameters are the initial concentration of the precursor, the initial citrate-to-gold molar ratio (or, equivalently, the quasi-equilibrium pH of the synthesis solution) and the solution temperature. From the seed correlation reported in Eq. (4.12), which holds only at 100 °C, we see that the first two parameters determine the size of the seed particles. The synthesis temperature, on the other hand, affects the values of the reaction rate constants and consequently of the selectivity of the precursor reduction and passivation reactions, as Eq. (3.27) reveals. Hence, taken together, the values of these three parameters determine the final size of the gold nanoparticles.

The particle size distribution predicted by our model is monodisperse owing to some assumptions on which the model is based. These assumptions are (1) the synthesis solution is perfectly mixed – the synthesis is assumed to occur in a perfectly-mixed batch reactor, (2) the seeds are assumed to have identical size (see Eq. (3.40)), and (3) the seed formation step is essentially decoupled from the growth step. Therefore, the predicted final particle size distribution is necessarily monodisperse. To obtain a polydisperse distribution, at least one of these assumptions has to be removed.

5. Conclusions

This work presented a new mathematical model for the description of the synthesis of gold nanoparticles via the citrate synthesis method. This method involves reducing tetrachloroauric acid with sodium citrate in an aqueous medium. In this medium, the precursor and reducing agent can exist in various forms by reacting with OH$^-$ and H$^+$, respectively. Furthermore, the system features several reactions and processes that occur in series and in parallel. Using the seed-mediated mechanism proposed by Wuithschick et al. (2015), we reported the steps describing the evolution of GNPs in the synthesis. Subsequently, we derived rate equations for the reactions involved in the reduction, passivation and growth steps, and proposed a method of calculating the seed diameter in the seed formation step. Then, we reported the synthesis model that describes how the components evolve with time, assuming that the pH value of the reaction mixture is constantly equal to its quasi-equilibrium value.

In this article, we solved the model for experimental conditions satisfying the criterion of initial values of the citrate-to-gold molar ratio equal to or greater than five. In this model, seed particles first form and then GNPs evolve from them. To determine the size of the seeds, we derived a correlation based on the initial conditions of the synthesis. We illustrated that the model predictions are sensitive to the value employed for the seed size. In the cases investigated, the model predictions agreed very well with the experimental data. In most of these cases, the growth process overrides the seed formation process in determining the final particle size; the more the amount of gold that passivates, the larger the final particle size is. At low pH values, nonetheless, we saw that seed sizes are larger, since the aggregation process is more vigorous.

Nomenclature

Roman alphabets

a	seed correlation parameter [–]
A	particle surface area per unit volume of solution [m^2/m^3]
B	seed correlation parameter [nm]
b	proportionality constant [–]
C	all the four species of citrate [–]
C_T, $C_{AuCl_4^-}$	concentration of tetrachloroauric ion [mol/m^3]
C_{Ct}	concentration of all citrate species [mol/m^3]
C_{H^+}	concentration of H$^+$ ions [mol/m^3]
C_{OH^-}	concentration of OH$^-$ ions [mol/m^3]
C_{Au}	concentration of gold in the particle phase [mol/m^3]
$C_{Au,max}$	maximum concentration of gold in the particle phase [mol/m^3]
C_{RA}	concentration of the reducing agent, which can be any of the species of citrates [mol/m^3]
C_{Pr1}	concentration of all other products from the reduction step, lumped together [mol/m^3]
C_{Pr2}	concentration of all other products from the growth step, lumped together [mol/m^3]
d	seed correlation parameter [–]
E_a	activation energy [J/mol]
$f(s)$	number of particles per particle-length per total volume of fluid-particle mixture [1/(m^3 m)]
G_s	linear growth rate [m/s]
k_0	pre-exponential factor [*Depends on application*]
k_r	rate constant for the reduction step [[m^3/mol]$^{1.85}$1/s]
k_p	rate constant for the passivation step [m^3/(mol s)]
k_g	rate constant for the growth step [m^4/(mol s)]
$K_{a,w}$	dissociation constant of water [–]
K_{Ri}'s	equilibrium constants of the speciation of citrate [–]
K_{Pi}'s	equilibrium constants of the speciation of the precursor [–]
l	reaction order of the precursor in the reduction step [–]
m_i	mass of species i [kg]
m_a	particles area shape factor [–]
m_v	particles volume shape factor [–]
n	reaction order of the reducing agent in the reduction step [–]
N_0	number of nuclei formed in the model developed by Kumar et al. per unit reactor volume [1/m^3]
N_P	final number of GNPs per unit reactor volume [1/m^3]
P	peak absorbance [–]
$Pr1$	by-products of the reduction step, lumped together [–]
$Pr2$	by-products of the growth step, lumped together [–]
Q	seed correlation parameter [nm]
r_r	rate of the reduction step [mol/(m^3 s)]
r_p	rate of the passivation step [mol/(m^3 s)]
r_g	rate of the growth step [mol/(m^3 s)]
r_m	particle mean radius [mol/(m^3 s)]
r_a	aggregate mean radius [mol/(m^3 s)]
R	universal gas constant
s	size [m]
s_0	nucleus diameter in the model of Kumar et al. [m]
s_s	seed diameter [m]
s_m	mean diameter with time [m]
s_f	final mean diameter [m]
S	selectivity of the reduction step over the passivation step [–]

t time [s]

$t_{r,0}$ time taken to reach the final peak absorbance along the x-axis [s]

t_s synthesis time [s]

T temperature [K]

V volume of synthesis solution [m^3]

x relative mole fraction of CtH_2^- at the quasi-equilibrium pH [−]

y relative mole fraction of CtH^{2-} at the quasi-equilibrium pH [−]

Y_i molar mass of species i [kg/mol]

Greek alphabets

ρ molar density of gold [mol/m^3]

τ_p reaction time for the passivation [s]

τ_g time for the growth step only in the citrate method [s]

Acknowledgments

Appendix A. Supplementary material

Supplementary data associated with this article can be found, in the online version, at https://doi.org/10.1016/j.ces.2018.06.046.

References

Abid, J.P., 2003. Laser Induced Synthesis and Nonlinear Optical Properties of Metal Nanoparticles Ph.D. Thesis. Ecole Polytechnique Federale de Lausanne, Lausanne, Switzerland.

Agunloye, E., Gavriilidis, A., Mazzei, L., 2017. A mathematical investigation of the Turkevich organizer theory in the citrate method for the synthesis of gold nanoparticles. Chem. Eng. Sci. 173, 275–286.

Chakraborty, A., Chakraborty, S., Chaudhuri, B., Bhattacharjee, S., 2016. Process engineering studies on gold nanoparticle formation via dynamic spectroscopic approach. Gold Bull. 49, 75. https://doi.org/10.1007/s13404-016-0183-7.

Cordero, B., Gómez, V., Platero-Prats, Ana E., Revés, Marc, Echeverría, Jorge, Cremades, Eduard, Barragán, Flavia, Alvarez, Santiago, 2008. Covalent radii revisited. Dalton Trans. (21), 2832–2838 https://doi.org/10.1039/b801115j.

Corma, A., Garcia, H., 2008. Supported gold nanoparticles as catalysts for organic reactions. Chem. Soc. Rev. 37, 2096–2126. https://doi.org/10.1039/B707314N.

Daniel, M., Astruc, D., 2004. Gold Nanoparticles: assembly, supramolecular chemistry, quantum-size-related properties, and applications toward biology, catalysis, and nanotechnology. Chem. Rev. 104, 293–346.

Dreaden, E.C., Austin, L.A., Mackey, M.A., El-Sayed, M.A., 2012. Size matters: gold nanoparticles in targeted cancer drug delivery. Ther Deliv. 3, 457–478. https://doi.org/10.4155/tde.12.21.

Fogler, H.S., 2004. Elements of Chemical Reaction Engineering. Prentice-Hall, Upper Saddle, New Jersey.

Frens, G., 1973. Controlled nucleation for the regulation of the particle size in monodisperse gold suspensions. Nature 241, 20.

Freund, P., Spiro, M., 1985. Colloidal catalysis: the effect of sol sizeand concentration. J. Phys. Chem. 89, 1074.

Hanes, G., Koeber, K., Kreuzbichler, I., Neu-Becker, U., Schwager, B., 1992. Gmelin Handbook of Inorganic and Organometalic Chemistry. Au Gold Supplement,. Springer-Verlag, Berlin.

Hashmi, A.S.K., Hutchings, G.J., 2006. Gold catalysis. Angew. Chem. Int. Ed. 45, 7896–7936. https://doi.org/10.1002/anie.200602454.

Hendel, T., Wuithschick, M., Kettemann, F., Birnbaum, A., Rademann, K., Polte, J., 2014. In situ determination of colloidal gold concentrations with UV-Vis spectroscopy: limitations and perspectives. Anal. Chem. 86 (22), 11115–11124.

Hvolbæk, B., Janssens, T.V., Clausen, B.S., Falsig, H., Christensen, C.H., Nørskov, J.K., 2007. Catalytic activity of Au nanoparticles. Nano Today 2, 14–18.

Ji, X.H., Song, X.N., Li, J., Bai, Y.B., Yang, W.S., Peng, X.G., 2007. Size control of gold nanocrystals in citrate reduction: the third role of citrate. J. Am. Chem. Soc. 129, 13939.

Kettemann, F., Birnbaum, A., Witte, S., Wuithschick, M., Pinna, N., Kraehnert, R., Rademann, K., Polte, J., 2016. Missing piece of the mechanism of the Turkevich method: the critical role of citrate protonation. Chem. Mater. 11, 4072–4081. https://doi.org/10.1021/acs.chemmater.6b01796.

Kumar, S., Kumar, R., Gandhi, K.S., 2007. Modeling of formation of gold nanoparticles by citrate method. Ind. Eng. Chem. Res. 46, 3128–3136. https://doi.org/10.1021/ie060672j.

Lane, L.A., Qian, X., Nie, S., 2015. SERS nanoparticles in medicine: from label-free detection to spectroscopic tagging. Chem. Rev. 115 (19), 10489–10529. https://doi.org/10.1021/acs.chemrev.5b00265.

Marchisio, D.L., Fox, R.O., 2013. Computational Models for Polydisperse Particulate and Multiphase Systems. Cambridge University Press, New York.

Matias, A.S., Carlos, F.F., Pedrosa, P., Fernandes, A.R., Baptista, P.V., 2017. Gold nanoparticles in molecular diagnostics and molecular therapeutics. In: Rai, M., Shegokar, R. (Eds.), Metal Nanoparticles in Pharma. Springer, New York, pp. 365–387.

Mersmann, A., 2001. Crystallization Technology Handbook. Dekker, New York.

Ojea-Jiménez, I., Campanera, J.M., 2012. Molecular modeling of the reduction mechanism in the citrate-mediated synthesis of gold nanoparticles. J. Phys. Chem. C 116, 23682–23691. https://doi.org/10.1021/jp305830p.

Pacławski, K., Streszewski, B., Jaworski, W., Luty-Błocho, M., Fitzner, K., 2012. Gold nanoparticles formation via Gold(III) chloride complex ions reduction with glucose in the batch and in the flow microreactor systems. Colloids Surfaces A: Physicochem. Eng. Aspects 413, 208–215. https://doi.org/10.1016/j.colsurfa.2012.02.050.

Peck, J.A., Tait, C.D., Swanson, B.I., Brown Jr, G.E., 1991. Speciation of aqueous gold (III) chlorides from ultraviolet/visible absorption and raman/resonance raman spectroscopies. Geochim. Cosmochim. Acta 55, 671–676.

Pines, E., Magnes, B.-Z., Lang, M.J., Fleming, G.R., 1997. Direct measurement of intrinsic proton transfer rates in diffusion-controlled reactions. Chem. Phys. Lett. 281 (4–6), 413–420.

Polte, J., Ahner, T.T., Delissen, F., Sokolov, S., Emmerling, F., Thünemann, A.F., Kraehnert, R., 2010. Mechanism of gold nanoparticle formation in the classical citrate synthesis method derived from coupled in situ XANES and SAXS evaluation. J. Am. Chem. Soc. 2010 (132), 1296–1301.

Ramkrishna, D., 2000. Population Balances. Academic Press, New York.

Serjeant, E.P., Dempsey, B., 1979. Ionisation Constants of Organic Acids in Aqueous Solution. International Union of Pure and Applied Chemistry (IUPAC). IUPAC Chemical Data Series No. 23. Pergamon Press, New York.

Sandler, S.I., 2006. Chemical, Biochemical, and Engineering Thermodynamics. John Wiley and Sons, New Jersey.

Stratakis, M., Garcia, H., 2012. Catalysis by supported gold nanoparticles: beyond aerobic oxidative processes. Chem. Rev. 112 (8), 4469–4506. https://doi.org/10.1021/cr3000785.

Turkevich, J., Stevenson, P., Hillier, J., 1951. A study of the nucleation and growth process in the synthesis of colloidal gold. Discuss. Faraday Soc. 11, 55.

Viswanatha, R., Sarma, A.A., 2007. Growth of Nanocrystals in Solution. In: Rao, C.N. R., Müller, A., Cheetham, A.K. (Eds.), Nanomaterials Chemistry: Recent Developments and New Directions. Wiley, pp. 139–170.

Wuithschick, M., Witte, S., Kettemann, F., Rademann, K., Polte, J., 2015. Turkevich in new robes: key questions answered for the most common gold nanoparticle synthesis. Phys. Chem. Chem. Phys. 17, 19895–19900. https://doi.org/10.1021/acsnano.5b01579.

Wulkow, M., Gerstlauer, A., Nieken, U., 2001. Modeling and simulation of crystallization processes using parsival. Chem. Eng. Sci. 56, 2575–2586. https://doi.org/10.1016/S0009-2509(00)00432-2.

Yang, X., Yang, M., Pang, B., Vara, M., Xia, Y., 2015. Gold nanomaterials at work in biomedicine. Chem. Rev. 115 (19), 10410–10488. https://doi.org/10.1021/acs.chemrev.5b00193.

Zabetakis, K., Ghann, W.E., Kumar, S., Daniel, M.-C., 2012. Gold Bull. 45, 203. https://doi.org/10.1007/s13404-012-0069-2.

Zhang, L., Wang, Y., Tong, L., Xia, Y., 2014. Synthesis of colloidal metal nanocrystals in droplet reactors: the pros and cons of interfacial adsorption. Nano Lett. https://doi.org/10.1021/nl501994q.

Zhou, W., Gao, X., Liu, D., Chen, X., 2015. Gold nanoparticles for in vitro diagnostics. Chem. Rev. 115 (19), 10575–10636. https://doi.org/10.1021/acs.chemrev.5b00100.